Network effects of subthalamic deep brain stimulation drive a unique mixture of responses in basal ganglia output

Mark D. Humphries[1,2] and Kevin Gurney[2]

[1]Group for Neural Theory, Department d'Etudes Cognitives, Ecole Normale Superieure, 29 rue d'Ulm, 75005 Paris, France
[2]Adaptive Behaviour Research Group, Department of Psychology, University of Sheffield, Western Bank, Sheffield, UK

Abstract

Deep brain stimulation (DBS) is a remarkably successful treatment for the motor symptoms of Parkinson's disease. High-frequency stimulation of the subthalamic nucleus (STN) within the basal ganglia is a main clinical target, but the physiological mechanisms of therapeutic STN DBS at the cellular and network level are unclear. We set out to begin to address the hypothesis that a mixture of responses in the basal ganglia output nuclei, combining regularized firing and inhibition, is a key contributor to the effectiveness of STN DBS. We used our computational model of the complete basal ganglia circuit to show how such a mixture of responses in basal ganglia output naturally arises from the network effects of STN DBS. We replicated the diversification of responses recorded in a primate STN DBS study to show that the model's predicted mixture of responses is consistent with therapeutic STN DBS. We then showed how this 'mixture of response' perspective suggests new ideas for DBS mechanisms: first, that the therapeutic frequency of STN DBS is above 100 Hz because the diversification of responses exhibits a step change above this frequency; and second, that optogenetic models of direct STN stimulation during DBS have proven therapeutically ineffective because they do not replicate the mixture of basal ganglia output responses evoked by electrical DBS.

Introduction

Deep brain stimulation (DBS) has proved to be a remarkably successful treatment for the motor symptoms of Parkinson's disease (Limousin *et al.*, 1995; Deep Brain Stimulation for Parkinson's Disease Study Group, 2001). High-frequency stimulation of the subthalamic nucleus (STN) within the basal ganglia has emerged as the main clinical target (Deep Brain Stimulation for Parkinson's Disease Study Group, 2001). The physiological mechanisms of therapeutic STN DBS at the cellular and network level are unclear (McIntyre *et al.*, 2004; McIntyre & Hahn, 2010).

One potential explanation is that high-frequency stimulation inhibits STN neuron firing (Beurrier *et al.*, 2001). However, although somatic inhibition of many STN neurons may occur (Beurrier *et al.*, 2001; Tai *et al.*, 2003; Moran *et al.*, 2011), their axons are probably stimulated to spike (Nowak & Bullier, 1998; Miocinovic *et al.*, 2006), others may fire somatically-generated spikes locked to the stimulation frequencies (Garcia *et al.*, 2003, 2005) and the firing patterns of others are modified (Moran *et al.*, 2011). Correspondingly, the basal ganglia output nuclei show elevated glutamate (Windels *et al.*, 2000) and firing rates (Hashimoto *et al.*, 2003; Bosch *et al.*, 2011; Moran *et al.*, 2011) during STN high-frequency stimulation. Subsequently, a theory has emerged that the key therapeutic action of DBS is regularization overwriting pathological activity (Perlmutter & Mink, 2006; Birdno *et al.*, 2007; Birdno & Grill, 2008). Previous theoretical work has shown how high-frequency stimulation of the STN could overwrite the pathological activity of basal ganglia output neurons by entraining their firing (Rubin & Terman, 2004; Hahn & McIntyre, 2010), and consequently return the target structures of the basal ganglia to normal operation by removing the deleterious effect of their pathological output (Rubin & Terman, 2004; Guo *et al.*, 2008; Dorval *et al.*, 2010).

A common result from studies of therapeutically effective STN DBS has received comparatively little attention: that STN DBS does not just overwrite, but rather causes a diversification of basal ganglia output. In the simplest manifestation, and consistent across species [human, Reese *et al.* (2011); primate, Hashimoto *et al.* (2003); rat, Shi *et al.* (2006)], the onset of therapeutic STN DBS causes a mixture of increased and decreased firing rates in the basal ganglia output nuclei. A plausible hypothesis is that this diversification of basal ganglia output, mixing regularized firing and inhibited neurons, underlies the effectiveness of STN DBS.

We set out to begin to address this hypothesis by extending our established computational model of the basal ganglia (Humphries *et al.*, 2006) to incorporate a simple model of DBS effects on STN neurons. Our first goal was to use the model to establish how such a mixture of responses can arise from the basal ganglia network, and whether the mixture of responses predicted by the model accurately reflected those found under therapeutic STN DBS in parkinsonian primates (Hashimoto *et al.*, 2003; Hahn *et al.*, 2008). Our second goal

Correspondence: M. D. Humphries, [1]Group for Neural Theory, as above.
E-mail: m.d.humphries@shef.ac.uk

was to seek whether, from the 'mixture of responses' perspective, the model could provide suggested resolutions to two DBS puzzles: why the clinically therapeutic frequency is above 100 Hz (Deep Brain Stimulation for Parkinson's Disease Study Group, 2001); and why optogenetic models of DBS failed to find a therapeutic effect when mimicking the direct activation of STN neurons (Gradinaru *et al.*, 2009).

Materials and methods

We first outline our computational model of the basal ganglia. A complete description is given in Humphries *et al.* (2006) – here we outline the pertinent features. Our model was explicitly of the rat basal ganglia, hence parameters such as transmission delays and neuron time constants were taken from the literature on the rat, and the tonic firing rates of the basal ganglia nuclei were fitted to those found in rat.

Basal ganglia circuitry

The basal ganglia are a group of inter-connected subcortical nuclei, which receive massive convergent input from most regions of the cortex, and output to targets in the thalamus and brainstem. Figure 1A illustrates the macro-architecture of the basal ganglia, showing the connections between the input nuclei (striatum and STN), output nuclei [substantia nigra pars reticulata and globus pallidus pars internus (GPi)], and internally-projecting globus pallidus pars externus

(GPe). Figure 1B illustrates the corresponding micro-architecture of the basal ganglia, implemented in the computational models (for detailed discussion, see Gurney *et al.*, 2001; Humphries *et al.*, 2006). In this model, the projections between the neural populations are topographically arranged to form a series of parallel loops (channels) running through the basal ganglia from input to output stages (Alexander & Crutcher, 1990; Hoover & Strick, 1993; Romanelli *et al.*, 2005).

For studying DBS effects, we used our basal ganglia model with 3 channels and 72 neurons per channel in each separate structure (striatum D1, striatum D2, STN, GPe and GPi), giving 1080 neurons in total. The connection probability between nuclei was set at $P = 0.25$ for connections within a channel, and $P = 0.25/3$ for diffuse connections across channels (STN projections to the GPi and GPe; local collaterals in the GPe and GPi). The massively convergent input from the striatum to its targets was accounted for by assigning the striatal connections a synaptic weight four times larger than all others.

Model neurons

The model used current-based integrate-and-fire neurons. The change in membrane potential V of each neuron was given by

$$\tau_m \frac{\mathrm{d}V}{\mathrm{d}t} = -V + R[I_{\text{syn}} + I_{\text{ion}} + I_{\text{DBS}}], \qquad (1)$$

with resistance R, membrane time constant τ_m, and driven by contributions from synaptic I_{syn}, ionic I_{ion}, and extrinsic I_{DBS} current
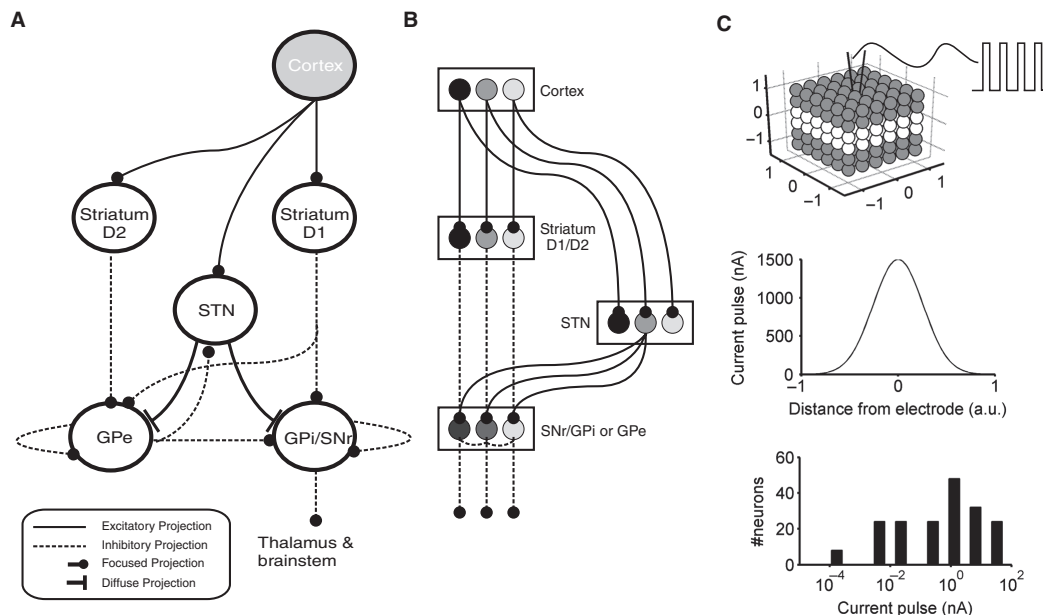

FIG. 1. The basal ganglia circuitry. (A) The basal ganglia macro-circuit. Cortical input reaches both the GABAergic striatum and glutamatergic STN. The striatum is divided into two populations of projection neurons, respectively expressing the D1- or D2-type dopamine receptors. The D1 population send their principal projections to the substantia nigra pars reticulata (SNr) and GPi; the D2 population send their principal projections to the GPe. Both the SNr/GPi and GPe receive input from the STN; the GPe reciprocates that projection. Both send local projections that inhibit neighbouring neurons. Constant inhibitory output from the SNr/GPi reaches widespread targets in the thalamus and brainstem. (B) The main circuit can be decomposed into two copies of an off-centre, on-surround network. Cortical inputs are topographically organized into separate groups that project to corresponding populations in the striatum and on through the SNr/GPi. In the SNr/GPi pathway, there is a balance of focussed inhibition from the striatum and comparatively diffuse excitation from the STN. In the D2–GPe pathway, a similar overlap of projections to the GPe exists, forming a second copy of this circuit. Three parallel loops are shown in both pathways; for clarity, full connectivity is only shown for the second loop. (C) Modelling DBS as a spread of effect. Top: we considered our STN as a six-per-edge cube of neurons, with each channel arranged as a $6 \times 6 \times 2$ layer of neurons, and with the DBS electrode placed at the cube's centre. Middle: the current injected into a model STN neuron with each DBS pulse was a Gaussian function of that neuron's distance from the electrode. The distance axis is in arbitrary units (a.u.), with ±1 indicating the edge of the volume. Shown for $I_{\text{max}} = 1500$ nA. Bottom: the resulting distribution of current injected into the model STN neurons for $I_{\text{max}} = 1500$ nA.

sources (in the present model only STN neurons received I_{DBS}, detailed below). A neuron fired a spike when $V \geq \theta$, and was reset to the resting potential $V_r =0$ mV; an absolute refractory period was then forced by stopping the solution of Eqn 1 for 2 ms. All neurons also had Gaussian noise added at every time step as a voltage deflection of V sampled from a Gaussian distribution of 0 ± 0.3 mV; this modelled both the numerous sources of noise (such as synaptic transmission failure) and the effect of unmodelled inputs to each neuron.

Synaptic input was modelled using GABAa synapses for all inhibitory connections and AMPA and N-methyl-D-aspartate (NMDA) synapses for all connections made by STN neurons and cortical inputs. Each synaptic event was modelled as a step-and-exponential-decay current. The current step was determined so that the average resulting post-synaptic potential peaked at ± 3 mV per input spike for GABAa and AMPA synapses, and 0.1 mV per input spike for NMDA synapses. The decay constants were set to standard values: AMPA, 2 ms; GABAa, 3 ms; and NMDA, 100 ms.

Although the model was based on point-neurons, we simulated a compartmental effect of GABAa synapses as the dendritic location of GABAergic synapses plays a major role in synaptic integration, and they are differentially distributed on target dendrites in the basal ganglia depending on the type of projection. For each inhibitory projection type (e.g. GPe–STN), the GABAa synapses on each target neuron were stochastically assigned to either a somatic, proximal, or distal pseudo-compartment, according to the synaptic distributions taken from data (Humphries *et al.*, 2006). GABAergic input to the proximal pseudo-compartment shunted synaptic input to the distal compartment; similarly, GABAergic input to the somatic pseudo-compartment shunted synaptic input to both distal and proximal compartments; shunting was simulated as a division of the incoming synaptic current in proportion to the number and strength of GABAa synapses in that pseudo-compartment. We had previously found (Humphries & Gurney, 2001) that this form of modelling GABAa shunting was essential for replicating the dual modes of slow bursting in the STN–GPe loop recorded *in vitro* (Plenz & Kitai, 1999).

The ionic contributions took two forms. First, all neurons received a tonic injection current; a positive current in STN, GPi, and GPe neurons phenomenologically modelled the current cycle underlying their tonic, pacemaker firing (Surmeier *et al.*, 2005). In Humphries *et al.* (2006), the positive currents were tuned to fit the tonic firing rates of these structures in awake rat; a negative current in striatal neurons phenomenologically modelled the strongly hyperpolarizing effect of their inward-rectifying potassium channel (Nisenbaum & Wilson, 1995). Second, STN neurons received an additional current source modelling the calcium-channel-dependent rebound bursting of these neurons (Beurrier *et al.*, 1999; Bevan *et al.*, 2002); the parameters were set mean values that allowed the model to replicate the duration and frequency of STN bursting *in vitro* (Beurrier *et al.*, 1999; Plenz & Kitai, 1999; Humphries & Gurney, 2001).

Mean values for τ_m and R were taken from published values for each neuron type (see Humphries *et al.*, 2006). In each instantiation of the model, values of τ_m and R for all neurons, and the burst-firing parameters for each STN neuron, were sampled from a Gaussian with an SD that was 10% of the mean value.

The parkinsonian model

Our basal ganglia model is able to simulate the effects of tonic dopamine on striatal projection neurons (separately for D1- and D2-receptor-expressing neurons), STN, and GPe, as detailed in Humphries *et al.* (2006). Here we examined DBS effects only under parkinsonian-like conditions, and so dopamine was absent from the

model throughout. In terms of our model parameters from Humphries *et al.* (2006), we set $\lambda_1 = \lambda_2 = 0$. In Humphries *et al.* (2006), we showed how changing the model from its normal tonic dopamine state to this parkinsonian state captured a broad range of known effects of dopamine loss on basal ganglia dynamics. First, loss of dopamine increased the transmission of cortical oscillatory activity through the STN and GPe loop, thus increasing the correlation of neuron firing in these structures, as observed in the 1-methyl-4-phenyl-1,2,3,6-tetrahydropyridine (MPTP) primate model and patients with Parkinson's disease (for review see Hammond *et al.*, 2007). Second, a combined dopamine and cortical lesion uncovered the residual slow bursting in the STN–GPe loop, as observed in 6-hydroxydopamine (6-OHDA) lesioned rats (Magill *et al.*, 2001). Third, loss of dopamine increased the proportion of substantia nigra pars reticulata∕GPi neurons that increase their firing rate during putative motor commands, as observed in MPTP primates (Leblois *et al.*, 2006b). Consequently, our simulations of STN DBS reported here were performed in a model consistent with a parkinsonian basal ganglia.

Modelling deep brain stimulation

We used a simple model of the effect of a DBS pulse on individual STN neurons, which attempted to qualitatively account for the spatial extent of tissue activated by DBS. Our starting assumption was that the change in extracellular voltage evoked by a DBS current pulse decays as a function of distance from the electrode (Rattay, 1999; Miocinovic *et al.*, 2006; Zhang & Grill, 2010), and thus induced current flow into the neuron also decays as a function of distance. Here we qualitatively model this by distributing the magnitude of DBS-evoked current injection as a Gaussian function of distance d from the electrode

$$I_{DBS} = I_{max} \exp[-(d/\sigma_d)^2]. \qquad (2)$$

We considered the model STN as cube of six, equally-spaced neurons per edge of unit length, with each channel a $6 \times 6 \times 2$ layer, and the DBS source as a point electrode placed in the centre (Fig. 1C). As not all of the STN is activated by DBS pulses (Miocinovic *et al.*, 2006), we set the Gaussian width at $\sigma_d = 0.1812$ to give a broad range of currents I_{DBS} across the model STN (an example distribution is plotted in Fig. 1C). As reported in the Results, we sought appropriate magnitudes for the maximum DBS-induced current flow I_{max} by fitting to DBS response data from MPTP primates (Hashimoto *et al.*, 2003). Unless otherwise stated, trains of DBS current pulses I_{DBS} were delivered at 130 Hz, with a width of 100 μs.

This simple model omits many proposed effects of DBS, including suppression of synaptic input, somatic inhibition of STN neurons, and direct activation of STN axons (McIntyre *et al.*, 2004). We noted, however, that the resulting mixture of firing rates in the STN (see, e.g. Fig. 2A) was consistent with the mixture of effects reported or predicted for STN high-frequency stimulation; some STN neurons showed stimulus-locked firing, replicating the DBS-locked somatic or axonal generation of STN spikes (Garcia *et al.*, 2003, 2005; Miocinovic *et al.*, 2006); some STN neurons were partially inhibited (Tai *et al.*, 2003; Moran *et al.*, 2011); some were completely inhibited (Miocinovic *et al.*, 2006; Moran *et al.*, 2011); and others showed synaptically-modulated firing patterns (Moran *et al.*, 2011). In our model, this mixture arises entirely from the interaction between the DBS pulses into STN neurons and the effects of the STN–GPe loop in the network, but undoubtedly the actions of DBS include suppression of synaptic input and direct activation of axons (Ranck, 1975; Rattay, 1999; McIntyre *et al.*, 2004; Miocinovic *et al.*, 2006).
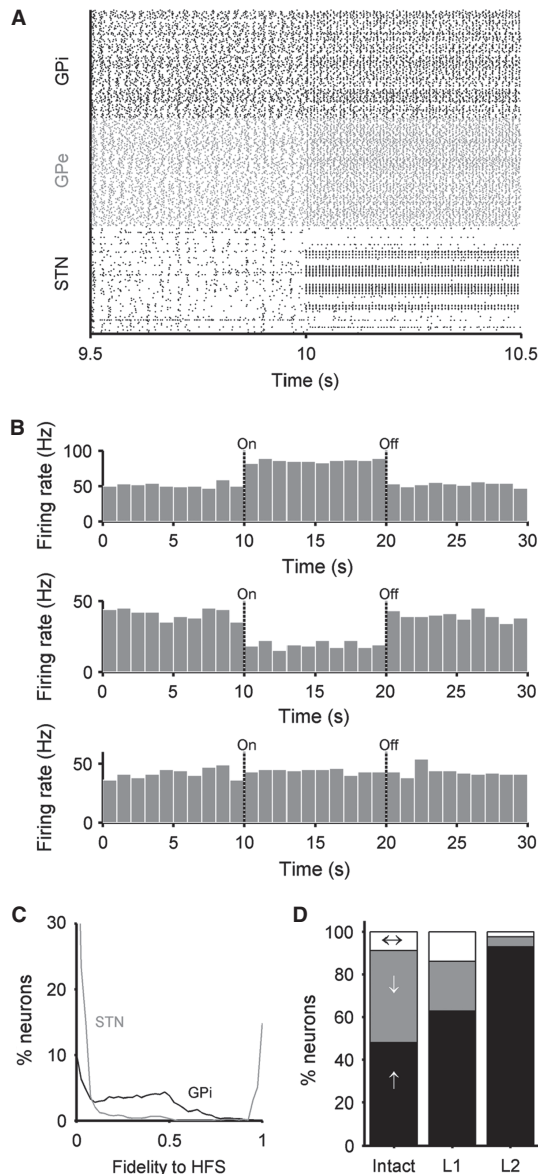
FIG. 2. Subthalamic high-frequency stimulation (HFS) evokes a mixture of responses in the output of the model basal ganglia. (A) Raster plot showing a 1 s snapshot of the outputs of all model STN, GPe, and GPi neurons in an example simulation. DBS (130 Hz, 100 μs width, I_{max} = 1500 nA) was switched on at 10 s. Some STN neurons became entrained to the stimulation, others were immediately silenced. (B) Example GPi neurons showing the mixture of firing rate responses to STN HFS: excitation (top), inhibition (middle), and no change (bottom). These three neurons are from the simulation in A. (C) Distribution of STN and GPi neuron fidelity to the 130 Hz stimulation of the STN. A fidelity of 1 indicates that the neuron fired after each DBS pulse; a fidelity of 0 indicates complete inhibition during the on-DBS epoch. (D) Distribution of firing rate responses to STN HFS over all neurons in the GPi: significant excitation (black), significant inhibition (grey), and no response (white). The three bars correspond to: the intact model (from A); L1, the same model with a lesion of the GPe to GPi pathway; and L2, the same model as L1 with a further lesion of local collaterals in the GPi.

We also used a simple model of optogenetic DBS, in which each STN neuron received the same size current pulse I_{DBS} to simulate the driving of the STN neurons by light-activated opening of channel-rhodopsin channels. Values for I_{DBS} were found by fitting to STN firing rate changes under optogenetic DBS (Gradinaru *et al.*, 2009), reported in the Results.

Simulations and statistics

All simulations using STN DBS were run for a total of 30 s, divided into three epochs: pre-DBS (10 s), on-DBS (10 s) and post-DBS (10 s). Rate histograms for single neurons were computed using 1 s bins. Changes in firing rate caused by STN stimulation were detected by computing a two-tailed Mann–Whitney *U*-test between the pre-DBS and on-DBS epochs; we took $P < 0.05$ as indicating a significant change in rate due to STN stimulation. The fidelity of firing to stimulation frequency was computed as the proportion of DBS pulses after which the neuron fired at least one spike before the next DBS pulse. The regularity of firing for each neuron was measured by its inter-spike interval (ISI) coefficient of variation (CV): ISI CV = SD (ISI)/mean (ISI).

For a detailed comparison with the data from the primate STN high-frequency stimulation study of Hashimoto *et al.* (2003), we used a 'models-as-animals' protocol (Humphries *et al.*, 2006; Humphries & Gurney, 2007b). Briefly, a typical electrophysiological study collects a total of T neurons across N animals and approximately C cells per animal; we matched this with T neurons from across N models and C neurons sampled per model. Each model has a different realization of the stochastic connectivity, and newly sampled distributions for R, τ_m, and the free parameters for I_{ion}, thus each represents a different animal. This approach circumvents issues of the differing statistical power and differing sampling of response classes with different total numbers of neurons T, and of the differing convergence of summary statistics depending on the combination of N and C (Humphries & Gurney, 2007b). In this way, we aimed to generate results, the statistical properties of which are similar to their experimental counterparts, thereby enabling statistically valid claims about the 'fit' between the model and the data.

Following our previous work (Humphries *et al.*, 2006), cortical input was generated as 72 spike trains per channel, connected to each STN and striatum neuron in that channel with a probability of 0.25. Input from the cortex was modelled under a variety of recording conditions. For replications of the data from awake, resting, head-fixed primates (Hashimoto *et al.*, 2003), we generated Poisson trains of 3 Hz (this input was used for all simulations unless otherwise specified). For optogenetic-like simulations in awake, freely-moving rats (Gradinaru *et al.*, 2009), we generated Poisson trains of 15 Hz. For tuning of the optogenetic DBS model to changes in STN firing rate, recorded in rat under isoflurane anaesthesia (Gradinaru *et al.*, 2009), we simulated the cortical slow wave at ~1 Hz induced by this anaesthetic (Ferron *et al.*, 2009), following our similar simulations of urethane anaesthesia (Humphries *et al.*, 2006). Every cortical train synchronously alternated between active up-states and silent down-states every 0.5 s; during each up-state, each train was assigned uniformly-spaced spikes at a rate f, sampled from a Gaussian of 24 ± 1.15 Hz, and each spike was then jittered by δ_t seconds, sampled from a Gaussian of 0 ± 0.25/f.

Results

Subthalamic nucleus high-frequency stimulation drives a mixture of responses in basal ganglia output

We begin by qualitatively illustrating the model's two main predictions for the network effects of STN high-frequency stimulation. First, that regular, high-frequency, pulsed, positive current stimulation of the STN drives a mixture of changes in the basal ganglia output nuclei. Second, that this mixture of responses is a network effect, arising from variations in the balance of glutamatergic input (from the STN) and GABAergic input to each neuron in the basal ganglia output nuclei.

Figure 2A shows the spike output of all model neurons in the STN, GPe, and GPi immediately preceding and following the onset of 130 Hz stimulation of the STN. The onset of stimulation entrained some STN neurons, whereas others were silenced, and others continued to fire irregularly (Fig. 2C). All of these effects were due entirely to the network response to the stimulation, as we did not explicitly model synaptic suppression, somatic inhibition, or any other source of inhibition to the STN other than synaptic input (which is not to say that those factors do not contribute to the effect of STN DBS). In the GPe and GPi, a subset of neurons also became entrained to their STN input, and increased their firing rate and regularity, but others showed reduced activity, and others did not change their firing rates. Figure 2B shows examples from the GPi of each firing rate response to STN stimulation.

Figure 2C shows that a subset of GPi neurons became tightly locked to the stimulation frequency and hence highly regularized in their output. Across the whole GPi, STN stimulation caused significant excitation and significant inhibition of responses in approximately equal proportions, with a small proportion of unresponsive neurons (Fig. 2D).

Although the excitatory responses were directly driven by STN firing, the equally prevalent inhibitory responses were a little counter-intuitive. By construction, we know that the model contains only three sources of GABAergic input to GPi neurons: the striatum, GPe, and local collaterals in the GPi. The striatum was barely active under the background cortical firing input, and was unaffected by STN stimulation. Lesioning the GPe to GPi pathway in the model reduced the proportion of inhibitory responses in the GPi (Fig. 2D). An additional lesion of the GPi local collaterals further decreased the proportion of inhibitory responses in the GPi (Fig. 2D). With all GABAergic sources accounted for, there remained only a small proportion of inhibitory responses in the GPi following STN high-frequency stimulation; thus, under this model of DBS, the silencing of some STN neurons makes a small contribution to the significant reduction of the firing rates of output neurons. The model thus shows that a mix of responses in basal ganglia output naturally arises from the network effects of STN high-frequency stimulation.

Using this model, we set out to answer the following. Is this the right mix of responses for therapeutically effective DBS in the STN? Does a ''mixture of response'' perspective offer an explanation for why STN DBS is therapeutically effective at greater than 100 Hz (Deep Brain Stimulation for Parkinson's Disease Study Group, 2001)? Does it offer some clues to why an optogenetic model of STN DBS might not work (Gradinaru *et al.*, 2009)?

Model replicates mix of rate and pattern responses during subthalamic nucleus deep brain stimulation in awake MPTP primate

We first assessed whether our simulated STN DBS created the mix of responses in the basal ganglia output corresponding to therapeutically effective DBS in the STN. To do so, we set out to replicate the data on neuron response changes from a study of STN DBS in the MPTP primate model (Hashimoto *et al.*, 2003; Hahn *et al.*, 2008). We chose this study as it is both the most complete data-set of changes in STN target nuclei under known therapeutic STN high-frequency stimulation and because there is a detailed analysis of individual neuron responses from Hahn *et al.* (2008). Our work here complemented that of Hahn & McIntyre (2010), who searched over parameters of a computational model of the STN–GPe–GPi circuit to fit the mean firing and burst rates from recordings of the MPTP state off-DBS, and then showed how simulated STN DBS changed both of these in

accord with the experimental data. We extended this by showing how a pre-existing model of the basal ganglia can, by changing only the I_{max} parameter of our DBS model, replicate both the changes in mean rate and regularity, and the mix of individual neuron responses.

We assessed the model's replication of STN stimulation-induced changes in both spike rate and regularity for different values of peak DBS current I_{max}. For replication of changes in firing rate, we measured: (i) the percentage change in mean rate from pre-DBS to on-DBS epochs from recorded neurons in the GPi and GPe, and (ii) the proportion of those recorded neurons that showed a significant increase, a significant decrease, and no change in firing rate. For the replication of changes in spike regularity, we measured the percentage changes in ISI CV from pre-DBS to on-DBS epochs from recorded neurons in the GPi. To compare with data, we first extracted individual neuron ISI CV responses from Fig. 2 of Hahn *et al.* (2008). In the experimental recordings, the mean ISI CV in the GPi did not significantly differ between pre-DBS and on-DBS epochs (Hahn *et al.*, 2008); however, individual neurons had large changes in regularity, with a mean increase of 40.4 ± 13.28% ($n = 12$) and mean decrease of −27 ± 2.91% ($n = 24$). Therefore, we assessed the replication of: (iii) the proportion of neurons that showed an increase and decrease of ISI CV; (iv) the mean percentage change in ISI CV for increasing neurons; (v) the mean percentage change in ISI CV for decreasing neurons; and (vi) the ensemble mean ISI CV not significantly differing between pre-DBS and on-DBS (two-tailed t-test, at $P = 0.05$). Thus, in total we assessed six measures of fit between GPi output in model and data.

For both rate and regularity, we assessed percentage changes because, as our model was explicitly of the rat basal ganglia, its tonic rates in the STN, GPe, and GPi were considerably less than those recorded in primate. Thus, we assessed magnitude changes, not exact values. To ensure similar statistics and sampling of distributions between models and data, we replicated the study design (see Materials and methods). The study of Hashimoto *et al.* (2003) used two monkeys, and Hahn *et al.* (2008) analysed a total of 20 GPe neurons and 36 GPi neurons recorded in both pre-DBS and on-DBS epochs. Thus, for each simulation of the study of Hashimoto *et al.* (2003), we used two instantiations of the model, sampling 10 GPe cells and 18 GPi cells from each.

Figure 3 shows that the model replicated all tested firing rate changes in the basal ganglia output during STN high-frequency stimulation: the percentage change in the mean rate of GPi neurons and the sampled mix of responses (increase, decrease, no change) in the GPi. These were simultaneously replicated across most tested values of I_{max}. The firing rate responses of the GPi in the MPTP primate were thus robustly well-fit. Figure 3 shows that, over a narrower range of I_{max} (∼1000–1500 nA), the model also simultaneously replicated the change in mean rate and sampled mix of responses in the GPe.

Figure 4 shows that the model replicated all tested GPi spike-train regularity changes during STN high-frequency stimulation: the mix of ISI CV responses (increase, decrease); the mean percentage change in ISI CV for neurons with increasing ISI CV; the mean percentage change for neurons with decreasing ISI CV; and the non-significant difference in mean ISI CV between pre-DBS and on-DBS epochs. Simultaneous replications of all regularity measures were robust across the lower range of I_{max} (∼500–1500 nA).

Across all fits to rate changes and mix of responses in the GPi and GPe, and to ISI CV changes and mix of responses in the GPi, the choice of $I_{max} = 1500$ nA was best able to simultaneously replicate all of these data properties (we quantify this statement in the next section). Thus, we used this value for further DBS simulations when assessing therapeutic effects.
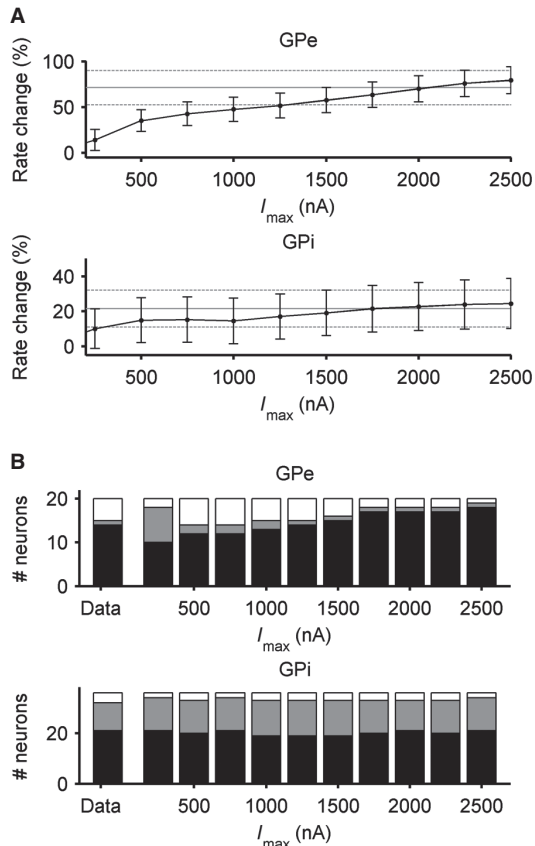
FIG. 3. The model replicates the magnitude and mixture of rate changes in a primate DBS study. (A) Percentage change in mean rate caused by high-frequency STN stimulation. Increasing the DBS current magnitude (I_{max}) caused a larger increase in mean firing rates in both the GPe and GPi. For $I_{max} \geq 1000$ nA, the model was able to reproduce closely the magnitude rate changes observed in both the GPe and GPi of primate. Model plotted as mean ± SEM. Grey lines give the target data: mean (solid) ± SEM (dashed) percentage change in rates in response to STN DBS in the MPTP primate model (Hashimoto *et al.*, 2003; Hahn *et al.*, 2008). (B) Mixture of responses in sampled neurons. Increasing I_{max} increased the number of excitatory responses (black) in the GPe, correspondingly decreasing the occurrence of both inhibitory responses (grey), and no change (white). By contrast, the mix of responses in the GPi was stable to the changes in I_{max}. The mix of responses observed under STN DBS in the MPTP primate model (Hashimoto *et al.*, 2003; Hahn *et al.*, 2008) was closely reproduced in the GPe over 500–1500 nA, and closely reproduced in the GPi for all tested currents. Data are given in the left-most bars.

The mixture of responses is robust to model variations

These results showed that the DBS-evoked mixture of rate and regularity responses, generated solely by the network of our model, was consistent with the mixture of rate and regularity responses seen under therapeutic STN DBS in primate. To further confirm the robustness of these results, we checked that plausible changes to the model still produced a mixture of responses in basal ganglia output, and replicated the primate data on STN DBS responses.

We checked three variants of the original model. The first variant omitted the discrete-channel architecture for the connections between basal ganglia structures. The presence of parallel loops running through the basal ganglia has strong support from anatomical studies (see, e.g. Alexander & Crutcher, 1990; Hoover & Strick, 1993; Romanelli *et al.*, 2005). Nonetheless, imposing discrete channels in our relatively small and densely connected model creates some correlation between the inputs to neurons in the same channel, which
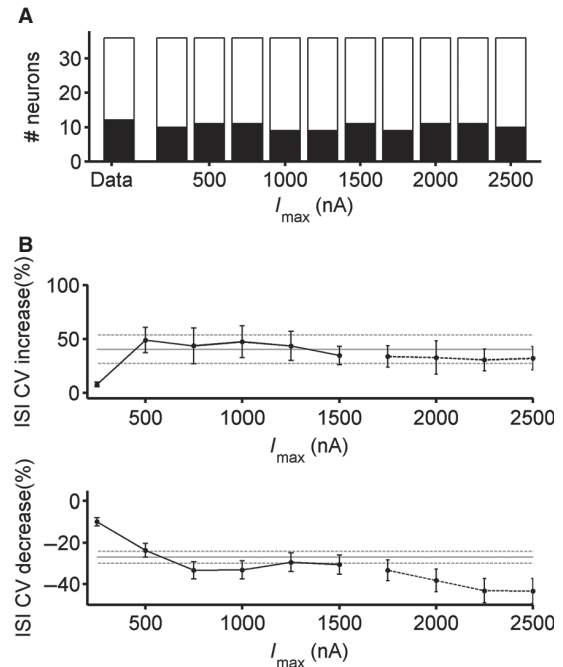

FIG. 4. The model replicated the magnitude and mixture of changes in GPi spike-train regularity from a primate DBS study. Regularity was measured by the CV of the ISIs. (A) The mixture of GPi neurons showing an increased (black) or decreased (white) ISI CV during STN high-frequency stimulation. For all tested maximum current size I_{max}, the ratio of CV response directions matched that of the data (Hashimoto *et al.*, 2003; Hahn *et al.*, 2008), given in the left-most bar. (B) Magnitude change in ISI CV caused by high-frequency STN stimulation. Top: mean percentage change for neurons with increased ISI CV. Bottom: mean percentage change for neurons with decreased ISI CV. For $I_{max} \leq 1500$ nA, the model was able to closely reproduce the same magnitude changes observed for both increasing and decreasing ISI CV neurons. Moreover, it was able to reproduce the non-significant difference of the overall mean ISI CV between pre-stimulation and on-stimulation epochs (black dashed line indicates range of I_{max} that gave a significant difference in mean ISI CV between pre-DBS and on-DBS epochs). Model data plotted as mean ± SEM. Grey lines: mean (solid) ± SEM (dashed) percentage change in ISI CV in response to STN DBS in the MPTP primate model (Hashimoto *et al.*, 2003; Hahn *et al.*, 2008).

could plausibly affect the results. For the no-channel model variant, every neuron connected with a probability of $P = 0.25/3$ to any neuron in each of its target structures. In this way, the expected number of connections between structures was exactly equivalent between the channel-based and no-channel models.

The second variant omitted the local axon collaterals in the GPi. As our model was originally of rat basal ganglia it explicitly modelled the substantia nigra pars reticulata as the main basal ganglia output nucleus, and consequently included the well-described local axon collaterals in that structure (Deniau *et al.*, 1982; Mailly *et al.*, 2003). However, beyond a brief note of their existence (Parent *et al.*, 2001), there has been little work establishing an equivalent network of local axon collaterals in the primate GPi. We thus checked that their omission did not affect our results. Finally, the third variant shortened the NMDA synaptic current decay constant to 50 ms, the lowest plausible value in the basal ganglia (Gotz *et al.*, 1997), to check that our results did not depend on prolonged excitation of GPe and GPi neurons by their STN inputs.

For each tested value of maximum DBS current I_{max}, we assessed each variant's error in reproducing the mixture of responses in the GPi and GPe (as in Fig. 3B), and each variant's ability to simultaneously fit all other measures of rate and regularity changes between pre-DBS

and on-DBS epochs. We assessed fits to the same five measures as for the original model: the GPi and GPe mean rate (as in Fig. 3A), mean GPi ISI CV increase and decrease (as in Fig. 4B), and the non-significant difference between all GPi ISI CVs in the pre-DBS and on-DBS epochs. For rate and ISI CV changes, we used a conservative criterion for a fit to the data: that the mean values for model and data were within 1 SEM, as illustrated by the error bars for the model and data plotted in Figs 3A and 4B.

Figure 5 shows that each model variant was able to reproduce the mixture of responses in GPi output evoked by STN DBS, with similar error to the original model, while also still being able to replicate all other tested measures of rate and regularity changes. Thus, the mixture of STN DBS evoked responses in basal ganglia output resulting from the basal ganglia network is highly robust to plausible changes in the model. We noted that the original model was best able to reproduce the mixture of responses in GPe output while still fitting all other measures. Consequently, we used this model for subsequent simulations.

Changing deep brain stimulation frequency changes the mixture of rate and regularity responses

A key unknown in understanding how DBS works is why the therapeutic frequency for the treatment of Parkinson's disease motor symptoms and tremor is normally above 100 Hz (Limousin *et al.*, 1995; Deep Brain Stimulation for Parkinson's Disease Study Group, 2001; Volkmann *et al.*, 2002). Here we show, using parameters for the DBS model established above, that our model predicts that basal ganglia output response patterns change dramatically with increasing DBS frequency, and a unique, stable balance of breadth of response and direction of response appears at therapeutic frequencies.

We assessed the firing rate and spike-train regularity changes of the model GPi neurons in response to a range of STN stimulation frequencies. We found that the mixture of firing rate responses
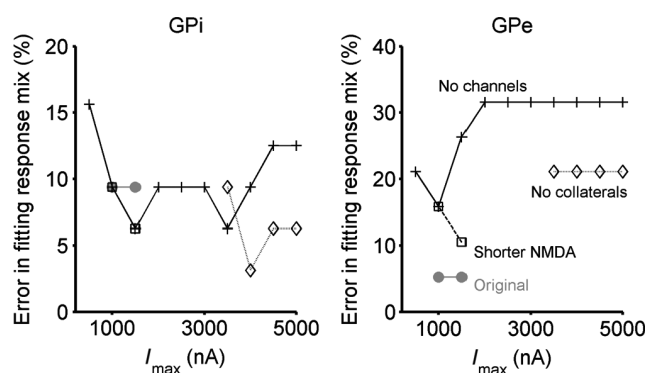

FIG. 5. Robustness of model replication of STN DBS evoked responses in the primate GPi and GPe (Hashimoto *et al.*, 2003; Hahn *et al.*, 2008). We plot the error for each model variant's fit to the mixture of responses in the GPi (left) and GPe (right) observed under STN DBS in the MPTP primate model (data in the left-most bars of Fig. 3B). Error is expressed as a percentage of the maximum error, which would be to assign all neurons to the smallest response category in the data. The plotted range of the lines shows the range of tested maximum DBS current I_{max} over which each model variant was also able to fit simultaneously all other measured GPi and GPe response properties in Figs 3 and 4. Under the conservative fitting criteria adopted here, the original basal ganglia model (grey circles) replicated all response properties between 1000 and 1500 nA. The model variants tested the effects of not imposing a discrete-channel architecture on the connections between structures (+), omitting the local collaterals in the GPi ($\diamond$), and reducing the time constant for decay of NMDA-evoked post-synaptic currents ($\square$).

(increase, decrease, no change) in the GPi became more stable above 100 Hz stimulation (Fig. 6A), with a marked step change in the proportion of inhibitory responses at 100 Hz stimulation (Fig. 6A, right). Figure 6B shows that the distribution of percentage firing rate changes across the GPi became strongly skewed above 100 Hz stimulation. Moreover, the distributions of changes were also stable for stimulation frequencies above 100 Hz (Fig. 6B, right). Thus, in addition to GPi neurons becoming strongly excited and entrained by STN stimulation, the larger proportion of significantly inhibitory responses included GPi neurons that became silenced only by stimulation above 100 Hz.

We found that the mixture of ISI CV direction changes in the GPi was not markedly altered by stimulation frequencies above 75 Hz (Fig. 6C). However, Fig. 6D shows that the distribution of ISI CV changes in the GPi became strongly asymmetric above 100 Hz. Moreover, the distributions of changes were also stable for stimulation frequencies above 100 Hz (Fig. 6D, right). Thus, although the proportion of GPi neurons showing increases and decreases in spike-train regularity did not markedly change at therapeutic stimulation frequencies, the magnitude of those changes did change.

Optogenetic model deep brain stimulation alters the response mix compared with the electrical deep brain stimulation model

Our results suggest that a specific mix of basal ganglia output rate and regularity changes is found under therapeutic STN DBS. We wondered if this observation could help to explain why using an optogenetic model of STN excitation by DBS failed to find any therapeutic effect in parkinsonian rats (Gradinaru *et al.*, 2009).

In an innovative use of recent developments in optogenetic technology, Gradinaru *et al.* (2009) addressed the controversy over the effect of high-frequency stimulation on the STN by driving spiking activity in channel-rhodopsin-expressing STN neurons with 130 Hz light pulses. However, they found that such unambiguous direct 130 Hz stimulation of STN neurons did not alleviate behavioural deficits in parkinsonian rats. These results present a serious challenge to the idea that elevated, regularized STN spiking activity – whether axonally or somatically induced – is key to the effectiveness of standard, electrical DBS.

We considered this difficulty from the perspective that a specific mix of responses in basal ganglia output is the main cause of STN DBS effectiveness. We noted that, in the study of Gradinaru *et al.* (2009), the excitation of the STN was exceptionally uniform. They estimated that almost all neurons (95.73 ± 1.96%) were infected with the channel-rhodopsin promoter Ca^{2+}/calmodulin-dependent protein kinases II (CaMKII), and thus likely to express the light-sensitive ion channels; further, they estimated that the wavelength of light used was able to penetrate the whole volume of the rodent STN ($\sim 0.7\ mm^3$) at a sufficient intensity to activate the light-sensitive ion channels. We hypothesized that this uniform excitation was the key to the ineffectiveness of an optogenetic DBS model.

To test this, we compared the output of our basal ganglia model under an optogenetic DBS model with the electrical DBS model established in the preceding sections. To mimic the uniform take up and light penetration, we modelled optogenetic-like stimulation of the STN by applying the same magnitude current pulse I_{DBS} to every STN neuron. We first estimated an appropriate magnitude of current pulse to mimic the optogenetic stimulation by fitting the change in STN firing rate during the optogenetic stimulation (Gradinaru *et al.*, 2009).

Gradinaru *et al.* (2009) reported an $\sim 100\%$ increase in STN firing rate in response to 130 Hz light stimulation, recorded in 6-OHDA-lesioned rats under isoflurane anaesthesia (whereas they tested the
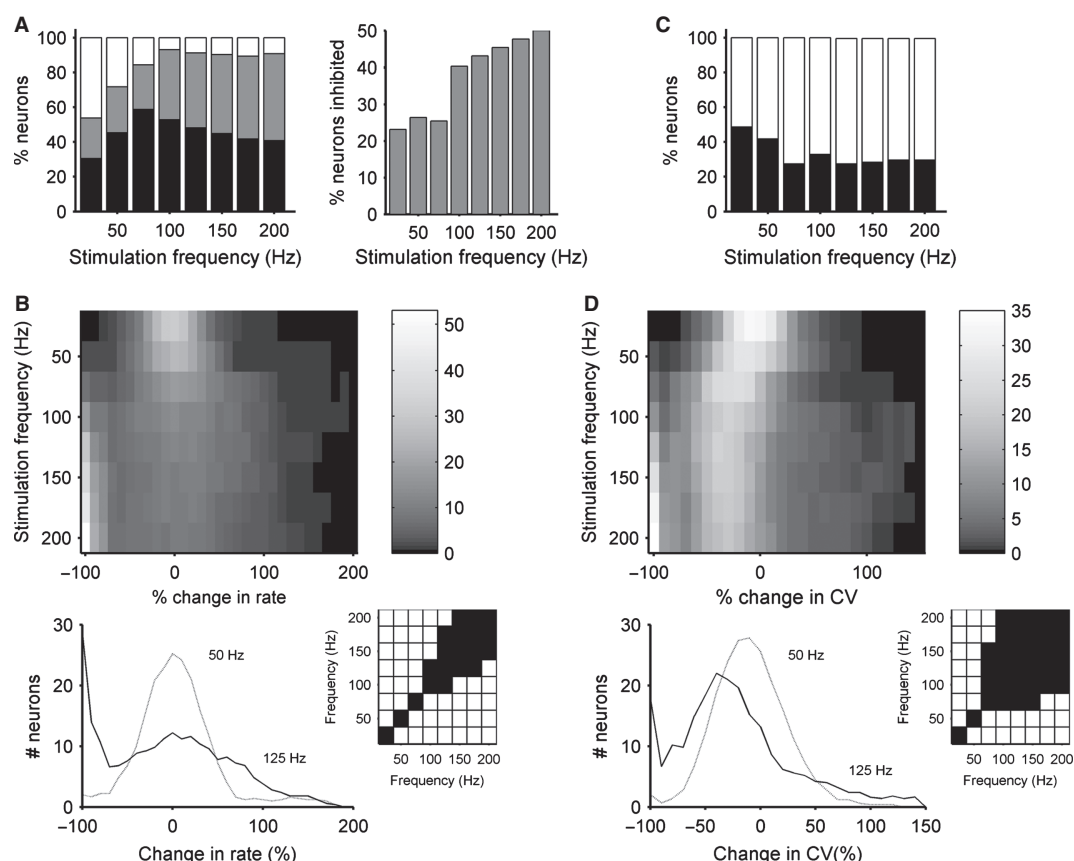
FIG. 6. High-frequency stimulation of the STN causes a unique pattern of changes in basal ganglia output. (A) Left: The mixture of GPi neurons showing an excitatory (black), inhibitory (grey), or no firing rate response at each stimulation frequency. Right: replotting the proportion of inhibitory responses at each stimulation frequency. (B) Top: the distribution of firing rate changes for each stimulation frequency. Colour intensity indicates number of neurons. Bottom: replotting the distributions at 50 and 125 Hz, illustrating the shift from symmetric to asymmetric distribution of firing rate changes above 100 Hz, including the jump in silenced neurons (−100% change). Right: significant (white) and non-significant (black) differences between the distributions of firing rate changes at each DBS frequency (Kolmogrov–Smirnov test, at $P = 0.05$). The non-significant differences illustrate the stability of the distributions for stimulation frequencies above 100 Hz. (C) The mixture of GPi neurons showing an increased (black) or decreased (white) ISI CV at each stimulation frequency. (D) Top: the distribution of changes in ISI CV for each stimulation frequency. Colour intensity indicates number of neurons. Bottom: replotting the distributions at 50 and 125 Hz, illustrating the shift from symmetric to asymmetric distribution of changes in ISI CV above 100 Hz. Right: significant (white) and non-significant (black) differences between the distributions of ISI CV changes at each DBS frequency (Kolmogrov-Smirnov test, at $P = 0.05$). The non-significant differences illustrate the stability of the distributions for stimulation frequencies above 100 Hz.

therapeutic effects of the optogenetic DBS model in awake, freely-moving rodents). Thus, we first found the appropriate magnitude of current pulse under isoflurane-like conditions, and then applied it to awake, freely-moving rat like conditions. Isoflurane systemically increases the efficacy of GABAa synapses (Krasowski & Harrison, 1999; Yamakura & Harris, 2000), and causes global slow-wave activity at ~1 Hz in the cortex (e.g. Ferron *et al.*, 2009). As these physiological effects of isoflurane are very similar to those of urethane (Rudolph & Antkowiak, 2004), we adopted a similar approach to our previous simulations of the effect of urethane on the basal ganglia (Humphries *et al.*, 2006); cortical input oscillated at 1 Hz with an average firing rate of 24 spikes/s (see Materials and methods), and we increased the GABAa synaptic weights by a factor of 1.5. Under this isoflurane-condition model, we tried a range of I_{DBS} uniformly applied at 130 Hz to every STN neuron during the on-DBS epoch. Following Gradinaru *et al.* (2009), for each tested I_{DBS} we computing the mean firing rate over five sampled STN neurons for the pre-DBS and on-DBS epochs. Figure 7A shows that $I_{DBS} = 45$ nA was able to accurately reproduce the reported increase in STN firing rate during optogenetic DBS.

We then compared the basal ganglia output responses for the optogenetic DBS model (with $I_{DBS} = 45$ nA) with our electrical DBS model [Eqn 2, using the best-fit to the data of Hashimoto *et al.* (2003) of $I_{max} = 1500$ nA, resulting in the distribution of I_{DBS} in Fig. 1C]. We ran 10 models of awake, freely-moving, 6-OHDA rodent basal ganglia (Gradinaru *et al.*, 2009), with each model run twice, once with the optogenetic DBS model and once with the electrical DBS model applied during the on-DBS epoch.

Figure 7B shows that the two DBS protocols differed markedly in their distribution of STN neuron fidelity to the DBS frequency, skewed towards high fidelity for the optogenetic DBS stimulation model, and bimodal in the electrical DBS model. We noted that this distribution of fidelity in the optogenetic DBS model is in keeping with the known fidelity of channel-rhodopsin-expressing neurons to regular, high-frequency, pulsed-light stimulation (Arenkiel *et al.*, 2007).

Our models showed that, with these differing STN response distributions, the optogenetic DBS and electrical DBS models had multiple differences in the mix of responses in the basal ganglia output. First, optogenetic DBS caused many more excitatory responses in the GPi than electrical DBS (Fig. 7C). Second, optogenetic DBS generally caused higher fidelity of GPi firing to the STN stimulation frequency, particularly in the regime of near 1 : 1 fidelity,
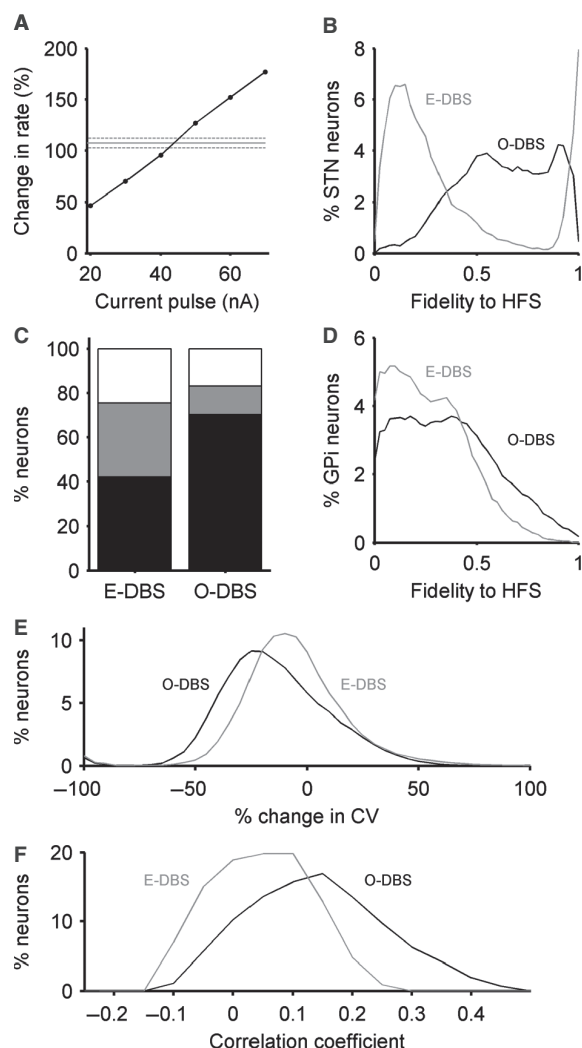
FIG. 7. Simulated STN optogenetic DBS and electrical DBS create different mixtures of responses in basal ganglia output. (A) Tuning the optogenetic DBS model. Mean increase in STN rate for a range of I_{DBS}, under simulated isoflurane-anaesthetized rat conditions. Grey lines give mean ± 2 SEM increase of STN firing during optogenetic DBS stimulation in the same conditions recorded by Gradinaru et al. (2009). (B) Fidelity of STN neuron firing to 130 Hz stimulation in the optogenetic DBS (O-DBS) and electrical DBS (E-DBS) models. (All data here and in subsequent panels taken from DBS applied in models of awake, freely-moving rat.) (C) The mixture of GPi neurons showing an excitatory (black), inhibitory (grey), or no (white) firing rate response to 130 Hz stimulation by optogenetic and electrical DBS models (mean over 10 models). (D) Fidelity of GPi neuron firing to the 130 Hz simulation of the STN in the O-DBS and E-DBS models. (E) The distribution of ISI CV changes in the GPi caused by each type of DBS model (mean over 10 models). (F) The distribution of spike correlations between neuron pairs caused by each type of DBS model. Correlation coefficients were computed between 200 randomly chosen pairs from the 10th model; their spike trains during the on-DBS epoch were binned at 2.5 ms. HFS, high-frequency stimulation.

than electrical DBS (Fig. 7D). Third, optogenetic DBS increased the regularity of GPi neuron firing more than electrical DBS (Fig. 7E). Consequently, with the increased fidelity and increased regularity of firing, optogenetic DBS caused more tightly-correlated firing between GPi neuron pairs than electrical DBS (Fig. 7F). Thus, our models show that optogenetic-like DBS and electrical-like DBS differ in their effects on the rate, regularity and correlation of the basal ganglia output.

Discussion

We set out to begin to address the hypothesis that a mixture of responses in the basal ganglia output nuclei, combining regularized firing and inhibition, is a key contributor to the effectiveness of STN DBS. We had two goals: first, to use our computational model of the complete basal ganglia circuit (Humphries et al., 2006) to understand how such a mixture of responses in basal ganglia output may arise from the network effects of STN DBS; and second, we sought whether, from this 'mixture of responses' perspective, the model could suggest resolutions to two DBS puzzles: the therapeutically effective range of frequencies, and the ineffectiveness of direct-activation optogenetic models of STN DBS. We showed that the model predicts a mixture of responses in the basal ganglia output arising as a natural consequence of the network effects of STN DBS. We replicated the diversification of responses recorded in a primate STN DBS study (Hashimoto et al., 2003; Hahn et al., 2008) to show that the model's predicted mixture of responses is consistent with therapeutic STN DBS. We then showed how, from this 'mixture of response' perspective, the model suggested the respective hypotheses for the two puzzles: that the mixture of responses in basal ganglia output undergoes a step change at therapeutic DBS frequencies; and that optogenetic DBS models failed because their uniform stimulation of the STN did not produce the putative therapeutically-effective mixture of responses evoked by standard, electrical DBS.

Subthalamic nucleus deep brain stimulation drives a mixture of responses in basal ganglia output

We have shown that STN DBS can induce a mix of excitatory and inhibitory responses in the basal ganglia output nuclei, with some neurons entrained to stimulation frequency and others strongly inhibited. This mix of responses arose purely from the basal ganglia network; simulated STN DBS only affected STN neurons, and we did not simulate other hypotheses for the distal action of DBS, including recruitment of passing axon fibres or antidromic activation of STN afferents (McIntyre et al., 2004; McIntyre & Hahn, 2010; Bosch et al., 2011). Nonetheless, this mix of responses in both spike rate and regularity accurately reflected those observed following therapeutic STN DBS in parkinsonian primates (Hashimoto et al., 2003; Hahn et al., 2008). Our model replicated the mixture of firing rate responses of GPe and GPi neurons, and the mean percentage changes in GPe and GPi firing rate following STN high-frequency stimulation. It also replicated the mixture of the changes in spike-train regularity of GPi neurons, the respective mean percentage increase and decrease, and the non-significant change in overall mean regularity following STN high-frequency stimulation. The model thus showed how the DBS results in this study were consistent with a purely network effect of STN DBS. We also showed that replication of these results was not dependent on a number of modelling assumptions (the imposition of a discrete-channel architecture, the presence of collaterals in the GPi, or the precise time-course of NMDA synaptic currents). Our results thus support the idea that a main contributor to the therapeutic effectiveness of STN DBS is its network effect, which creates a mixture of responses in the basal ganglia output through the balance of STN-originating excitation and GPe-originating inhibition arriving at the GPi (Kita et al., 2005; McIntyre & Hahn, 2010; Bosch et al., 2011; Reese et al., 2011).

Subthalamic nucleus deep brain stimulation frequency determines the mixture of responses

The therapeutically-effective frequency of STN DBS is typically above 100 Hz in human patients (Deep Brain Stimulation for

Parkinson's Disease Study Group, 2001). Although stimulation frequencies in this range may enable STN neuron firing to track the DBS pulses (Garcia *et al.*, 2005), our model suggests a network-based explanation for this range. We found that increasing stimulation frequency to the effective range for DBS caused a step change in the basal ganglia output's response characteristics. The distributions of both spike-rate and spike regularity changes became strongly skewed above 100 Hz, reflecting the appearance of GPi neurons that were strongly entrained or silenced by STN DBS. Moreover, the proportion of inhibitory responses in the GPi non-linearly increased at 100 Hz. The model's results are thus consistent with a transition from symmetric to asymmetric effects of STN DBS on basal ganglia output at therapeutic frequencies.

Optogenetic deep brain stimulation may alter the mixture of responses

Gradinaru *et al.* (2009) recently used optogenetics to address the controversy over the effect of DBS on the STN. They tested the hypothesis that DBS directly activates STN neurons, by driving spiking activity in channel-rhodopsin-expressing STN neurons with 130 Hz light pulses. However, they found that such direct 130 Hz stimulation of STN neurons did not alleviate behavioural deficits in parkinsonian rat models, strongly challenging the idea that elevated and regularized STN spiking activity alone underpins the effectiveness of standard, electrical DBS. To address this, we simulated optogenetic DBS as a uniform stimulation of STN neurons, with a stimulating current pulse tuned to fit the reported change in STN firing rate following the onset of optogenetic DBS (Gradinaru *et al.*, 2009). The model showed that optogenetic DBS stimulation was unable to provide the same diversity of responses in basal ganglia output as the electrical DBS stimulation. Optogenetic DBS predominantly caused an increased firing rate in GPi output, and a corresponding increase in regular, stimulation-tracking, firing and in the correlation of GPi neuron output. If the effectiveness of STN DBS indeed rests on a particular mixture of responses, then this may explain why a direct-excitation optogenetic model of STN DBS, causing uniform stimu-lation of STN neurons, did not result in the effective alleviation of motor symptoms in the parkinsonian rat (Gradinaru *et al.*, 2009). Thus, in addition to other possible contributors to the therapeutic failure of the optogenetic model of STN DBS (such as millisecond different time-scales of STN neuron synchronization by electrical and light stimulation), our model offers a novel network-based hypothesis.

Why then, from this perspective, did Gradinaru *et al.* (2009) find that optogenetic high-frequency stimulation of either all layer 5 cortical terminals in the STN or layer 5 neurons in the motor cortex could alleviate the parkinsonian motor symptoms? As they noted, these results are consistent with the therapeutic effect of electrical STN DBS arising from antidromic activation of these cortical neurons. However, we note that both stimulations could cause a non-uniform excitation of STN neurons. In both cases, whether stimulating all cortical afferents from layer 5 or just those with somas in the motor cortex layer 5, these make up only a subset of glutamatergic projections to STN neurons. A major glutamatergic input arises from the parafascicular thalamus (Bevan *et al.*, 1995), and others from across the upper brainstem (Bevan & Bolam, 1995). Thus, the stimulated terminals or neurons will be differentially distributed across the STN, with some STN neurons strongly innervated by layer 5 cortical neurons and others more weakly innervated. Moreover, as the optogenetic stimulation in both cases was driving synaptic input to the STN and not direct spiking, it is probably more susceptible to modulation by GABAergic input from the GPe. Thus, we speculate

that optogenetic high-frequency stimulation of layer 5 terminals or somas has a similar effect on STN neurons to the spreading current model of electrical DBS used here, thus resulting in the mixture of basal ganglia output responses corresponding to therapeutic DBS.

How might a mixture of responses to deep brain stimulation restore function?

We have used computational models here to generate mechanistic hypotheses for the action of STN high-frequency stimulation on basal ganglia output nuclei, and for the effectiveness of DBS. The next, crucial step will be to address if and why such a mix of responses is key to the restorative effect of DBS. We comment on three perspectives here. First, from the perspective that DBS restores function to the targets of the basal ganglia by output regularization. Elegant studies by Rubin and colleagues (Rubin & Terman, 2004; Guo *et al.*, 2008) and Dorval *et al.* (2010) have provided compelling demonstrations of how, by regularizing basal ganglia output to the thalamus, STN DBS may improve the transmission of the excitatory inputs of thalamo-cortical neurons. Our results are consistent with STN DBS regularizing the output of a subset of GPi neurons, and hence the reinstatement of thalamic information transfer, but our results also point to the silencing of a substantial number, and a mixture of responses in the rest of the basal ganglia output. The studies of thalamo-cortical relay fidelity have typically considered the effect of one or a few GPi inputs, on an isolated thalamo-cortical cell, relaying one type of input (a pulsed current), and using one model of error in thalamic information transfer (a 1 : 1 spike-locking regime). Consequently, in the context of a full basal ganglia-thalamo-cortical circuit or of other models of thalamic information transfer to the cortex (such as the necessary synchronization of thalamo-cortical neurons) (Bruno & Sakmann, 2006; Bruno, 2011), it may turn out that regularizing all basal ganglia output simply overwrites one form of pathological activity with another, artificially generated form. Indeed, a prediction of our model is that the optogenetic DBS model failed to alleviate parkinsonian motor symptoms (Gradinaru *et al.*, 2009) because it over-regularized the basal ganglia output. Thus, one possibility is that a balance of regularization and inhibition amongst the basal ganglia output neurons is necessary for the restoration of thalamic relay fidelity.

Second, we consider how DBS might restore function to targets of the basal ganglia output through the seemingly paradoxical removal of inhibition. The dominant theory of basal ganglia function is that they operate by disinhibition – signalling the selection of motor pro-grammes by selectively reducing their tonic inhibitory output to their target structures (Mink, 1996; Redgrave *et al.*, 1999; Hikosaka *et al.*, 2000). The therapeutic success of STN DBS, and its activation of basal ganglia output nuclei (Hashimoto *et al.*, 2003; Shi *et al.*, 2006; Bosch *et al.*, 2011; Moran *et al.*, 2011; Reese *et al.*, 2011), is a considerable challenge to this theory (Nambu, 2008), as how can stimulating the STN alleviate motor symptoms, when it increases the activity of basal ganglia output, and consequently increases, not reduces, their tonic inhibition of target structures? Our results suggest a resolution, i.e. that, through its network effect, STN DBS actually generates widespread, permanent inhibition of much basal ganglia output, including the silencing of a number of neurons (see Fig. 6A, right). Consequently, STN DBS would permanently reduce the tonic inhibition of a subset of neurons in the basal ganglia target structures, allowing them to respond to their other inputs. Moreover, we showed that this inhibition of basal ganglia output was consistent with the effects of therapeutically-effective STN DBS on the primate GPi (Hashimoto *et al.*, 2003; Hahn *et al.*, 2008). Thus, our model shows

how both information transfer through and disinhibition of basal ganglia target nuclei could be reinstated by STN DBS.

Finally, a view-point strangely lacking from theoretical STN DBS studies to date is how it might re-enable information flow through the basal ganglia from the striatum to its outputs (Hammond *et al.*, 2007). That is, in both the above perspectives, STN DBS restores function to target structures through permanently altering basal ganglia output, but they do not address if or how STN DBS restores function to the basal ganglia through reinstating control over that output. Our results suggest a preliminary observation. In our model, the mixture of responses to STN DBS amongst the basal ganglia output neurons is underpinned by each neuron's balance of excitatory input from the STN and GABAergic input from the GPe and local collaterals. By reinstating the dominance of inhibition over some basal ganglia output neurons and the dominance of excitation over others, STN DBS may thus allow phasic inhibitory input from the striatum to again modulate basal ganglia outflow, and reinstate basal ganglia computation (Mink, 1996; Redgrave *et al.*, 1999; Gurney *et al.*, 2001; Humphries *et al.*, 2006; Leblois *et al.*, 2006a). Understanding if such a mixture of responses is indeed key to the restoration of function in the basal ganglia is our next challenge.

Acknowledgements

Abbreviations

6-ODHA, 6-hydroxydopamine; CV, coefficient of variation; DBS, deep brain stimulation; GPe, globus pallidus pars externus; GPi, globus pallidus pars internus; ISI, inter-spike interval; MPTP, 1-methyl-4-phenyl-1,2,3,6-tetrahydropyridine; NMDA, *N*-methyl-D-aspartate; STN, subthalamic nucleus.

References

Alexander, G.E. & Crutcher, M.D. (1990) Functional architecture of basal ganglia circuits: neural substrates of parallel processing. *Trends Neurosci.*, **13**, 266–272.

Arenkiel, B.R., Peca, J., Davison, I.G., Feliciano, C., Deisseroth, K., Augustine, G.J., Ehlers, M.D. & Feng, G. (2007) In vivo light-induced activation of neural circuitry in transgenic mice expressing channelrhodopsin-2. *Neuron*, **54**, 205–218.

Beurrier, C., Congar, P., Bioulac, M. & Hammond, C. (1999) Subthalamic nucleus neurons switch from single spike-activity to burst-firing mode. *J. Neurosci.*, **19**, 599–609.

Beurrier, C., Bioulac, B., Audin, J. & Hammond, C. (2001) High-frequency stimulation produces a transient blockade of voltage-gated currents in subthalamic neurons. *J. Neurophysiol.*, **85**, 1351–1356.

Bevan, M.D. & Bolam, J.P. (1995) Cholinergic, GABAergic, and glutamate-enriched inputs from the mesopontine tegmentum to the subthalamic nucleus in the rat. *J. Neurosci.*, **15**, 7105–7120.

Bevan, M.D., Francis, C.M. & Bolam, J.P. (1995) The glutamate-enriched cortical and thalamic input to neurons in the subthalamic nucleus of the rat: convergence with GABA-positive terminals. *J. Comp. Neurol.*, **361**, 491–511.

Bevan, M.D., Magill, P.J., Hallworth, N.E., Bolam, J.P. & Wilson, C.J. (2002) Regulation of the timing and pattern of action potential generation in rat subthalamic neurons in vitro by GABA-A IPSPs. *J. Neurophysiol.*, **87**, 1348–1362.

Birdno, M.J. & Grill, W.M. (2008) Mechanisms of deep brain stimulation in movement disorders as revealed by changes in stimulus frequency. *Neurotherapeutics*, **5**, 14–25.

Birdno, M.J., Cooper, S.E., Rezai, A.R. & Grill, W.M. (2007) Pulse-to-pulse changes in the frequency of deep brain stimulation affect tremor and modeled neuronal activity. *J. Neurophysiol.*, **98**, 1675–1684.

Bosch, C., Degos, B., Deniau, J.-M. & Venance, L. (2011) Subthalamic nucleus high-frequency stimulation generates a concomitant synaptic excitation-inhibition in substantia nigra pars reticulata. *J. Physiol.*, **589**, 4189–4207.

Bruno, R.M. (2011) Synchrony in sensation. *Curr. Opin. Neurobiol.*, **21**, 701–708.

Bruno, R.M. & Sakmann, B. (2006) Cortex is driven by weak but synchronously active thalamocortical synapses. *Science*, **312**, 1622–1627.

Deep Brain Stimulation for Parkinson's Disease Study Group (2001) Deep-brain stimulation of the subthalamic nucleus or the pars interna of the globus pallidus in Parkinson's disease. *N. Engl. J. Med.*, **345**, 956–963.

Deniau, J.M., Kitai, S.T., Donoghue, J.P. & Grofova, I. (1982) Neuronal interactions in the substantia nigra pars reticulata through axon collaterals of the projection neurons. An electrophysiological and morphological study. *Exp. Brain Res.*, **47**, 105–113.

Dorval, A.D., Kuncel, A.M., Birdno, M.J., Turner, D.A. & Grill, W.M. (2010) Deep brain stimulation alleviates parkinsonian bradykinesia by regularizing pallidal activity. *J. Neurophysiol.*, **104**, 911–921.

Ferron, J.-F., Kroeger, D., Chever, O. & Amzica, F. (2009) Cortical inhibition during burst suppression induced with isoflurane anesthesia. *J. Neurosci.*, **29**, 9850–9860.

Garcia, L., Audin, J., D'Alessandro, G., Bioulac, B. & Hammond, C. (2003) Dual effect of high-frequency stimulation on subthalamic neuron activity. *J. Neurosci.*, **23**, 8743–8751.

Garcia, L., D'Alessandro, G., Fernagut, P.-O., Bioulac, B. & Hammond, C. (2005) Impact of high-frequency stimulation parameters on the pattern of discharge of subthalamic neurons. *J. Neurophysiol.*, **94**, 3662–3669.

Gotz, T., Kraushaar, U., Geiger, J., Lubke, J., Berger, T. & Jonas, P. (1997) Functional properties of AMPA and NMDA receptors expressed in identified types of basal ganglia neurons. *J. Neurosci.*, **17**, 204–215.

Gradinaru, V., Mogri, M., Thompson, K.R., Henderson, J.M. & Deisseroth, K. (2009) Optical deconstruction of parkinsonian neural circuitry. *Science*, **324**, 354–359.

Guo, Y., Rubin, J.E., McIntyre, C.C., Vitek, J.L. & Terman, D. (2008) Thalamocortical relay fidelity varies across subthalamic nucleus deep brain stimulation protocols in a data-driven computational model. *J. Neurophysiol.*, **99**, 1477–1492.

Gurney, K., Prescott, T.J. & Redgrave, P. (2001) A computational model of action selection in the basal ganglia I: a new functional anatomy. *Biol. Cybern.*, **85**, 401–410.

Hahn, P.J. & McIntyre, C.C. (2010) Modeling shifts in the rate and pattern of subthalamopallidal network activity during deep brain stimulation. *J. Comput. Neurosci.*, **28**, 425–441.

Hahn, P.J., Russo, G.S., Hashimoto, T., Miocinovic, S., Xu, W., McIntyre, C.C. & Vitek, J.L. (2008) Pallidal burst activity during therapeutic deep brain stimulation. *Exp. Neurol.*, **211**, 243–251.

Hammond, C., Bergman, H. & Brown, P. (2007) Pathological synchronization in Parkinson's disease: networks, models and treatments. *Trends Neurosci.*, **30**, 357–364.

Hashimoto, T., Elder, C.M., Okun, M.S., Patrick, S.K. & Vitek, J.L. (2003) Stimulation of the subthalamic nucleus changes the firing pattern of pallidal neurons. *J. Neurosci.*, **23**, 1916–1923.

Hikosaka, O., Takikawa, Y. & Kawagoe, R. (2000) Role of the basal ganglia in the control of purposive saccadic eye movements. *Physiol. Rev.*, **80**, 953–978.

Hoover, J.E. & Strick, P.L. (1993) Multiple output channels in the basal ganglia. *Science*, **259**, 819–821.

Humphries, M.D. & Gurney, K.N. (2001) A pulsed neural network model of bursting in the basal ganglia. *Neural Netw.*, **14**, 845–863.

Humphries, M.D. & Gurney, K. (2007a) Deep brain stimulation of the subthalamic nucleus causes paradoxical inhibition of output in a computational model of the ''parkinsonian'' basal ganglia. In *2007 Neuroscience Meeting Planner* Program No. 622.9. Society for Neuroscience, San Diego, CA, USA.

Humphries, M.D. & Gurney, K. (2007b) A means to an end: validating models by fitting experimental data. *Neurocomputing*, **70**, 1892–1896.

Humphries, M.D., Stewart, R.D. & Gurney, K.N. (2006) A physiologically plausible model of action selection and oscillatory activity in the basal ganglia. *J. Neurosci.*, **26**, 12921–12942.

Kita, H., Tachibana, Y., Nambu, A. & Chiken, S. (2005) Balance of monosynaptic excitatory and disynaptic inhibitory responses of the globus pallidus induced after stimulation of the subthalamic nucleus in the monkey. *J. Neurosci.*, **25**, 8611–8619.

Krasowski, M.D. & Harrison, N.L. (1999) General anaesthetic actions on ligand-gated ion channels. *Cell. Mol. Life Sci.*, **55**, 1278–1303.

Leblois, A., Boraud, T., Meissner, W., Bergman, H. & Hansel, D. (2006a) Competition between feedback loops underlies normal and pathological dynamics in the basal ganglia. *J. Neurosci.*, **26**, 3567–3583.

Leblois, A., Meissner, W., Bezard, E., Bioulac, B., Gross, C.E. & Boraud, T. (2006b) Temporal and spatial alterations in GPi neuronal encoding might contribute to slow down movement in Parkinsonian monkeys. *Eur. J. Neurosci.*, **24**, 1201–1208.

Limousin, P., Pollak, P., Benazzouz, A., Hoffmann, D., Bas, J.F.L., Broussolle, E., Perret, J.E. & Benabid, A.L. (1995) Effect of parkinsonian signs and symptoms of bilateral subthalamic nucleus stimulation. *Lancet*, **345**, 91–95.

Magill, P.J., Bolam, J.P. & Bevan, M.D. (2001) Dopamine regulates the impact of the cerebral cortex on the subthalamic nucleus-globus pallidus network. *Neuroscience*, **106**, 313–330.

Mailly, P., Charpier, S., Menetrey, A. & Deniau, J.M. (2003) Three-dimensional organization of the recurrent axon collateral network of the substantia nigra pars reticulata neurons in the rat. *J. Neurosci.*, **23**, 5247–5257.

McIntyre, C.C. & Hahn, P.J. (2010) Network perspectives on the mechanisms of deep brain stimulation. *Neurobiol. Dis.*, **38**, 329–337.

McIntyre, C.C., Grill, W.M., Sherman, D.L. & Thakor, N.V. (2004) Cellular effects of deep brain stimulation: model-based analysis of activation and inhibition. *J. Neurophysiol.*, **91**, 1457–1469.

Mink, J.W. (1996) The basal ganglia: focused selection and inhibition of competing motor programs. *Prog. Neurobiol.*, **50**, 381–425.

Miocinovic, S., Parent, M., Butson, C.R., Hahn, P.J., Russo, G.S., Vitek, J.L. & McIntyre, C.C. (2006) Computational analysis of subthalamic nucleus and lenticular fasciculus activation during therapeutic deep brain stimulation. *J. Neurophysiol.*, **96**, 1569–1580.

Moran, A., Stein, E., Tischler, H., Belelovsky, K. & Bar-Gad, I. (2011) Dynamic stereotypic responses of basal ganglia neurons to subthalamic nucleus high-frequency stimulation in the parkinsonian primate. *Front. Syst. Neurosci.*, **5**, 21.

Nambu, A. (2008) Seven problems on the basal ganglia. *Curr. Opin. Neurobiol.*, **18**, 595–604.

Nisenbaum, E.S. & Wilson, C.J. (1995) Potassium currents responsible for inward and outward rectification in rat neostriatal spiny projection neurons. *J. Neurosci.*, **15**, 4449–4463.

Nowak, L.G. & Bullier, J. (1998) Axons, but not cell bodies, are activated by electrical stimulation in cortical gray matter. I. Evidence from chronaxie measurements. *Exp. Brain Res.*, **118**, 477–488.

Parent, M., Levesque, M. & Parent, A. (2001) Two types of projection neurons in the internal pallidum of primates: single-axon tracing and three-dimensional reconstruction. *J. Comp. Neurol.*, **439**, 162–175.

Perlmutter, J.S. & Mink, J.W. (2006) Deep brain stimulation. *Annu. Rev. Neurosci.*, **29**, 229–257.

Plenz, D. & Kitai, S.T. (1999) A basal ganglia pacemaker formed by the subthalamic nucleus and external globus pallidus. *Nature*, **400**, 677–682.

Ranck, J.B. (1975) Which elements are excited in electrical stimulation of mammalian central nervous system: a review. *Brain Res.*, **98**, 417–440.

Rattay, F. (1999) The basic mechanism for the electrical stimulation of the nervous system. *Neuroscience*, **89**, 335–346.

Redgrave, P., Prescott, T.J. & Gurney, K. (1999) The basal ganglia: a vertebrate solution to the selection problem? *Neuroscience*, **89**, 1009–1023.

Reese, R., Leblois, A., Steigerwald, F., Pötter-Nerger, M., Herzog, J., Mehdorn, H.M., Deuschl, G., Meissner, W.G. & Volkmann, J. (2011) Subthalamic deep brain stimulation increases pallidal firing rate and regularity. *Exp. Neurol.*, **229**, 517–521.

Romanelli, P., Esposito, V., Schaal, D.W. & Heit, G. (2005) Somatotopy in the basal ganglia: experimental and clinical evidence for segregated sensorimotor channels. *Brain Res. Brain Res. Rev.*, **48**, 112–128.

Rubin, J.E. & Terman, D. (2004) High frequency stimulation of the subthalamic nucleus eliminates pathological thalamic rhythmicity in a computational model. *J. Comput. Neurosci.*, **16**, 211–235.

Rudolph, U. & Antkowiak, B. (2004) Molecular and neuronal substrates for general anaesthetics. *Nat. Rev. Neurosci.*, **5**, 709–720.

Shi, L.-H., Luo, F., Woodward, D.J. & Chang, J.-Y. (2006) Basal ganglia neural responses during behaviorally effective deep brain stimulation of the subthalamic nucleus in rats performing a treadmill locomotion test. *Synapse*, **59**, 445–457.

Surmeier, D.J., Mercer, J.N. & Chan, C.S. (2005) Autonomous pacemakers in the basal ganglia: who needs excitatory synapses anyway? *Curr. Opin. Neurobiol.*, **15**, 312–318.

Tai, C.-H., Boraud, T., Bezard, E., Bioulac, B., Gross, C. & Benazzouz, A. (2003) Electrophysiological and metabolic evidence that high-frequency stimulation of the subthalamic nucleus bridles neuronal activity in the subthalamic nucleus and the substantia nigra reticulata. *FASEB J.*, **17**, 1820–1830.

Volkmann, J., Herzog, J., Kopper, F. & Deuschl, G. (2002) Introduction to the programming of deep brain stimulators. *Mov. Disord.*, **17**(Suppl 3), S181–S187.

Windels, F., Bruet, N., Poupard, A., Urbain, N., Chouvet, G., Feuerstein, C. & Savasta, M. (2000) Effects of high frequency stimulation of subthalamic nucleus on extracellular glutamate and GABA in substantia nigra and globus pallidus in the normal rat. *Eur. J. Neurosci.*, **12**, 4141–4146.

Yamakura, T. & Harris, R.A. (2000) Effects of gaseous anesthetics nitrous oxide and xenon on ligand-gated ion channels. Comparison with isoflurane and ethanol. *Anesthesiology*, **93**, 1095–1101.

Zhang, T.C. & Grill, W.M. (2010) Modeling deep brain stimulation: point source approximation versus realistic representation of the electrode. *J. Neural Eng.*, **7**, 066009.